Frontiers in Bioscience Landmark

Front. Biosci. (Landmark Ed) **2023**; 28(5): 92
https://doi.org/10.31083/j.fbl2805092

Original Research

Changes in Starburst Amacrine Cells in Mice with Diabetic Retinopathy

Jae-Rim Son[1], Myung-Jun Lee[1,2], Chang-Jin Jeon[1,2,3,*]

[1]Department of Biology, School of Life Sciences, BK21 FOUR KNU Creative BioResearch Group, College of Natural Sciences, Kyungpook National University, 41566 Daegu, Republic of Korea
[2]Research Institute for Dok-do and Ulleung-do Island, Department of Biology, School of Life Sciences, Kyungpook National University, 41566 Daegu, Republic of Korea
[3]Brain Science & Engineering Institute, Kyungpook National University, 41944 Daegu, Republic of Korea
*Correspondence: cjjeon@knu.ac.kr (Chang-Jin Jeon)
Academic Editor: Adrian Gericke
Submitted: 22 February 2023 Revised: 15 March 2023 Accepted: 20 April 2023 Published: 15 May 2023

Abstract

Background: Neurodegenerative diseases, such as diabetic retinopathy (DR) and glaucoma, induce retinal neuron loss. Acetylcholine-containing cholinergic neurons, known as starburst amacrine cells (SACs), play critical roles in the generation of precise neuronal activity in the retina and are located in the inner nuclear layer (INL, conventional) and ganglion cell layer (GCL, displaced). **Methods**: This study investigated the loss of and morphological changes in SACs in the retinas of streptozotocin (STZ)-induced diabetic and insulin-deficient C57BL/6-Tg(pH1-siRNA$_{insulin}$/CMV-hIDE)/Korl (IDCK) mice. SACs were immunocytochemically localized with anti-choline acetyltransferase (ChAT) antibody, and ChAT-labeled cells in the INL and GCL in the control and experimental groups were counted along the central vertical meridian in the whole-mounted retina using conventional fluorescent or confocal microscopes. **Results**: ChAT-immunoreactive (IR) neurons in STZ-induced diabetic mouse retina decreased by 8.34% at 4–6 weeks and by 14.89% at 42 weeks compared with the control group. Localized ChAT-IR neuron counts in the retinas of 20-week-old IDCK mice were 16.80% lower than those of age-matched control mice. Cell body deformation and aggregation were detected in the retinas of mice with DR. Single-cell injection experiments revealed the loss and deformation of dendritic branches in ChAT-IR neurons in DR. All ChAT-IR neurons expressed the calcium-binding protein calretinin, whereas no ChAT-IR neuron colocalized with calbindin-D28K or parvalbumin. **Conclusions**: Our results revealed that the neurodegenerative effects of the loss and deformation of ChAT-IR neurons can provide a reference for future study of this disease.

Keywords: starburst amacrine cells; diabetic retinopathy; streptozotocin; choline acetyltransferase; calcium-binding proteins; immunocytochemistry

1. Introduction

Diabetic retinopathy (DR) is a major complication of diabetes that can lead to progressive vision loss and blindness [1–4]. Approximately one-third of individuals with diabetes develop DR, the treatment of which requires multiple options due to its complex and multifactorial pathogenesis [3,5]. Hyperglycemia, which induces superoxide production and oxidative stress, plays a central role in the development of vascular alterations [6,7]. Diabetic microvascular complications typically include neuropathy, nephropathy, and retinopathy, whereas macrovascular complications include cerebrovascular, cardiovascular, and peripheral complications [8,9]. DR is also a strong predictor of microvascular and macrovascular complications [8,10,11].

DR has been classified into two types: non-proliferative diabetic retinopathy (NPDR) and proliferative diabetic retinopathy (PDR). NPDR occurs in the first stage of DR and is characterized by altered vascular permeability, basement membrane thickening, pericytes loss, and acellular capillary formation. NPDR can be further divided into three types based on its progression: mild NPDR, moderate NPDR, and severe NPDR. PDR is an advanced stage of DR and is characterized by neovascular complications and may lead to retinal detachment. In any stage of DR, diabetic macular oedema may develop due to the accumulation of exudative fluid in the macula [1,3,12,13].

A growing body of research have reported that neurodegeneration plays a significant role in the development of DR [6,14]. DR is a highly specific neurovascular complication accompanied by progressive damage to retinal neurons, including such as photoreceptors, horizontal, bipolar, amacrine, and retinal ganglion cells (RGCs), and glial cells, such as Müller cells, astrocytes, and microglia [2,15]. Previous studies have shown that the loss of retinal cells is associated with increased apoptosis, decreased thickness, and cell density reduction [16–21]. Neurodegeneration in DR occurs in early stages even before vascular lesions can be detected [3,22,23]. However, there is still a debate over whether microvasculopathy causes neurodegeneration or vice versa or if they are mutually independent [3,22,24,25].

Streptozotocin (STZ), initially isolated from *Streptomyces achromogenes*, is a naturally occurring chemical agent that is particularly toxic to the insulin-producing beta cells in the pancreatic islet and is the most prominent diabetogenic chemical compound in diabetes research [26]. Many studies have used STZ-induced diabetic animal models, especially mouse and rat models of DR [16–18,20,27–30]. For example, periodic progression of cellular and vascular lesions in STZ-induced DR has been reported [27]. In mice with STZ-induced diabetes, the number of cells in the ganglion cell layer (GCL) was reduced [16,18]. In addition, in rats with STZ-induced diabetes, retinal cell apoptosis was increased, whereas the total retinal thickness was decreased [17,20,28]. The relationship between vascular damage and neuronal changes, such as apoptosis of retinal neurons, has also been investigated using mice with STZ-induced diabetes [29]. Basement membrane thickening of arterial and venous capillaries has been observed in the retina of rats with STZ-induced diabetes [30].

Starburst amacrine cells (SACs) release two neurotransmitters, the excitatory neurotransmitter acetylcholine and the inhibitory neurotransmitter gamma-aminobutyric acid (GABA). SACs are also called cholinergic amacrine cells because they are the only retinal cells that release acetylcholine [31–34]. SACs are distributed regularly in the retina [34–37]. SACs in the GCL are called displaced SACs or OFF-SACs, and those in the inner nuclear layer (INL) are called conventional SACs or ON-SACs. SACs play several important roles, including a major role in the detection of motion images in the retina [38,39].

Calcium ions participate in several important neuronal actions, and calcium-binding proteins (CBPs) are known to mediate the functions of calcium [40,41]. Calbindin-D28K (CB), calretinin (CR), and parvalbumin (PV) are CBPs distributed in a large subpopulation of retinal neurons [42,43]. The CBP expression of choline acetyltransferase (ChAT)-immunoreactive (IR) neurons differs among animals. For example, ChAT-IR neurons express CB in the lungfish retina [44], bat retina [35], ground squirrel retina [45], and human and marmoset retina [46], whereas CR is expressed in the lungfish retina [44], rat retina [47], and ground squirrel retina [45]. However, ChAT-IR neurons only express PV in the ground squirrel retina [45] and rabbit retina [48].

The death of several retinal cell types with the progression of DR and the loss of ChAT-IR neurons in the retinas of 24-week-old $Ins2^{AKITA}$ diabetic mice has been demonstrated [17,49]. However, there are no reports on the loss and changes in SACs in the retinas of STZ-induced diabetic mice or transgenic diabetic models in the early or late stages of DR. Hence, we aimed to investigate the loss of and morphological changes in SACs in the early (4–6 weeks) and late stages (42 weeks) of DR in mice with STZ-induced diabetes. Moreover, we examined 20-week-old insulin-deficient C57BL/6-Tg(pH1-siRNA$_{insulin}$/CMV-hIDE)/Korl (IDCK) mouse retinas and compared the results with previously reported findings in $Ins2^{AKITA}$ diabetic mice. In addition, we investigated whether ChAT-IR neurons in the mouse retina express CB, CR, or PV. The findings are expected to provide information about the loss of and morphological changes in SACs in diabetic mouse retina and clarify the expressions of CB, CR, and PV in ChAT-IR neurons in the mouse retina.

2. Materials and Methods

2.1 Animals

All experiments involving animals were approved by the Animal Care and Use Committee of Kyungpook National University (permission no. 2020-0158). Animals were group housed under a 12-h light:12-h dark cycle until used for studies. Temperature and humidity levels in animal housing facilities ranged from 23 °C to 26 °C and from 45% to 65%, respectively.

2.1.1 STZ-Induced Diabetic Mice and Experimental Design

Adult mice (C57BL/6J, 8–10 weeks old, weighing 20–30 g) were examined. After 4 h of fasting, we measured their weight and blood glucose levels and randomly categorized the animals into experimental and control groups. Experimental mice were intraperitoneally administered 6 mg/ml STZ dissolved in 50 mM sodium citrate buffer (pH 4.5), and control animals were intraperitoneally administered 50 mM sodium citrate buffer (pH 4.5) in reference to standard protocol of previous study [27]. We calculated the amount of injection solution at ratio of 40 mg/kg of weight of each mouse and injected via intraperitoneal injection using 1 mL syringe. The aforementioned process was repeated for 5 days. After injection, we checked the weight and fasting blood glucose level of each mouse every 5 days. Blood was obtained from the tail vein. Two weeks after the injection, mice with blood glucose levels >250 mg/dL were considered diabetic (Table 1).

2.1.2 IDCK Mice

IDCK mice were obtained from the National Institute of Food and Drug Safety Evaluation (Cheongju, Korea). IDCK mice with blood glucose levels >240 mg/dL were used as experimental mice, and age-matched C57BL/6N mice with blood glucose levels <200 mg/dL were used as control mice (Table 1) [50].

2.1.3 Tissue Preparation

C57BL/6J mice at 4–6 and 42 weeks after STZ injection and IDCK mice at 20 weeks after birth were euthanized with isoflurane inhalation (5% in O_2), and their eyes were immediately enucleated. The retinas were carefully isolated from the eyecups in a fixative [4% paraformaldehyde in 0.1 M phosphate buffer (PB) pH 7.4 containing 0.002% calcium chloride]. The detached retinas were stored for 2 h in

Table 1. Average blood glucose levels in the experimental and control groups.

Animals	Duration (week)	Group	Number	BGL (mg/dL)
STZ injected mice (C57BL/6J mice)	4–6	Diabetic	3	450.00 ± 132.10
		Control	3	178.33 ± 12.50
	42	Diabetic	3	404.67 ± 171.30
		Control	3	160.33 ± 12.66
IDCK mice (C57BL/6N mice)	20	Diabetic	3	265.00 ± 32.92
		Control	3	166.67 ± 34.02

BGL, blood glucose level; STZ, streptozotocin; IDCK, insulin-deficient C57BL/6-Tg(pH1-siRNA$_{insulin}$/CMV-hIDE)/Korl.

the same fixative. The fixed retinas were washed with 0.1 M PB.

2.2 Fluorescence Immunocytochemistry

Retinal whole mounts were processed free-floating in small vials at room temperature with gentle agitation. With three rinses in ice-cold 0.1 M PB between each step, the retinas were processed as follows: (1) freezing and thawing three times for better antibody penetration; (2) preincubation in 1% sodium borohydride for 20–30 min; (3) incubation in 0.1 M PB with 4% normal serum from the host of secondary antibody with 0.5% Triton X-100 for 1 day; (4) incubation in the primary antiserum in blocking solution for 3 days; (5) incubation in the secondary antiserum in blocking solution for 1 day; and (6) staining of the nuclei of the retinas with DAPI (1:1000). The primary antibodies used in this study were rabbit anti-CB (1:250, Sigma-Aldrich, St. Louis, MO, USA), rabbit anti-CR (1:200, Sigma-Aldrich), rabbit anti-PV (1:250, Swant, Burgdorf, Bern, Switzerland), and goat anti-ChAT (1:200, Millipore, Burlington, MA, USA). For CB, CR, and PV, fluorescein isothiocyanate (FITC)-conjugated anti-rabbit IgG (Jackson ImmunoResearch Inc., Baltimore, PA, USA) secondary antibody was used. To identify ChAT, FITC-conjugated goat anti-rabbit IgG secondary antibody (Millipore) and Cy3- conjugated donkey anti-goat IgG (Jackson ImmunoResearch Inc.) secondary antibodies were used.

2.3 Single-Cell Injection

The procedures for single-cell injection following immunocytochemistry have been described in our previous reports [51–53]. Immunocytochemistry before the single-cell injection procedure was performed without Triton X-100 because this detergent can influence the diffusion of the dye in the neuronal membrane. The fixed tissues were incubated in a 1:200 dilution of goat anti-ChAT (Millipore) primary antibody in 0.1 M PB for 2 h at room temperature and then incubated in a 1:50 dilution of FITC-conjugated donkey anti-goat IgG secondary antibody (Jackson ImmunoResearch Inc.) in 0.1 M PB for 2 h at room temperature after three rinses with 0.1 M PB. The dish containing the immunolabeled retinal tissue was placed on a microscope stage, and FITC-labeled cholinergic neurons were viewed under a Zeiss 40× Plan Achroplan (NA 0.80) water immersion lens and Zeiss filter set 09 (excitation, 450–490 nm; emission, 515 nm). Single ChAT-labeled cells in the GCL were randomly selected. The cells were filled by iontophoretically passing a positive current of 5–20 nA through a micropipette containing a 1% solution of the lipophilic dye DiI (Molecular Probes, Eugene, OR, USA). DiI-filled cells were viewed using Zeiss filter set 20 (excitation, 540–552 nm; emission, 575–640 nm), and the optimal filling time was usually 15–30 min. We only injected cells in the mid-periphery of the retina (1.0–1.7 mm peripheral to the optic disc) because the dendritic field size varies with retinal eccentricity. After several cells in the retina were filled, the tissue was fixed for 2 h in 4% paraformaldehyde. The tissue was washed three times in 0.1 M PB, coverslipped with Vectashield (Vector Laboratories, Burlingame, CA, USA), and sealed with nail polish.

2.4 Microscopy and Quantitative Analysis

We counted ChAT-IR neurons manually in whole-mounted retinas from the center to the periphery. As the density of retinal neurons changes with eccentricity, we carefully chose counting areas by positioning at the same retinal regions between control and experimental mice. We counted cells in fourteen sample areas at 300 μm intervals throughout the dorsoventral meridians of the retina with 200 × 200 μm^2 fields from three retina each of control and experimental mice. Cell density was expressed as the number of ChAT-IR neurons/mm^2. The ratios were evaluated statistically using paired student *t*-test between control and experimental mice. ChAT-IR neuron distribution and double-labeling percentage were examined using a Zeiss Axioplan microscope (Carl Zeiss Meditec, Inc., Jena, Germany). Fluorescence images were photographed with a Zeiss Axioplan microscope using a 40× objective or Zeiss LSM800 laser-scanning confocal microscope (Carl Zeiss Meditec, Inc.) using a 20× or 40× objective.

3. Results

3.1 Distribution of ChAT-IR Neurons in DR

The typical distribution of ChAT-IR neurons in the mouse retina has been described in our previous study [19].

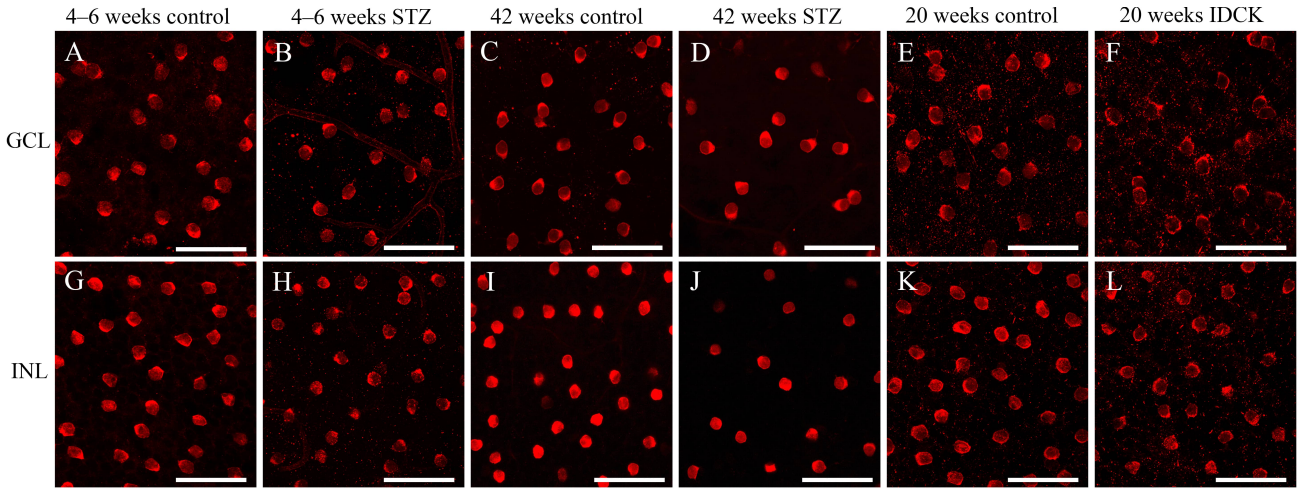

Fig. 1. High-power photomicrographs of the ChAT-IR neuron distribution in the mouse retina. (A–F) ChAT-IR neurons in the GCL of the mouse retina. (G–L) ChAT-IR neurons in the INL of the mouse retina. (A,G) ChAT-IR neurons in mice in the control group at 4–6 weeks after STZ injection. (B,H) ChAT-IR neurons in mice in the experimental group at 4–6 weeks after STZ injection. (C,I) ChAT-IR neurons in mice in the control group at 42 weeks after STZ injection. (D,J) ChAT-IR neurons in mice in the experimental group at 42 weeks after STZ injection. (E,K) ChAT-IR neurons in 20-week-old C57BL/6N mice in the control group. (F,L) ChAT-IR neurons in 20-week-old IDCK mice in the experimental group. The density of ChAT-IR neurons was reduced in all experimental groups compared with the control groups. STZ, streptozotocin; IDCK, insulin-deficient C57BL/6-Tg(pH1-siRNA$_{insulin}$/CMV-hIDE)/Korl; GCL, ganglion cell layer; INL, inner nuclear layer; ChAT, choline acetyltransferase; IR, immunoreactive. Scale bar = 50 μm.

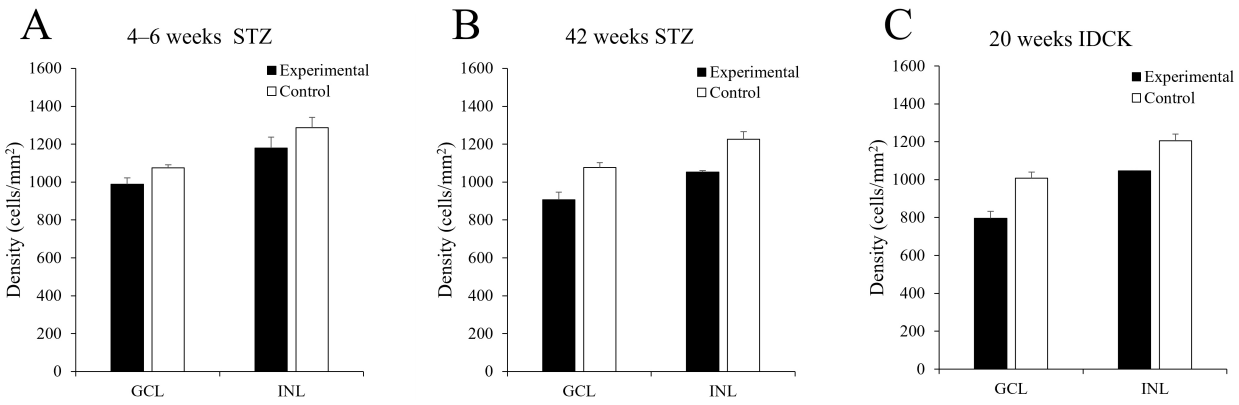

Fig. 2. Histogram showing mean density of ChAT-IR neurons in the mouse retina. (A) At 4–6 weeks after STZ injection, ChAT-IR neuron counts decreased by 8.15% (GCL) and 8.48% (INL) in the experimental group compared with the control group. (B) At 42 weeks after STZ injection, ChAT-IR neuron counts decreased by 15.73% (GCL) and 14.14% (INL) in the experimental group compared with the control group. (C) In 20-week-old IDCK mouse retinas, ChAT-IR neuron counts decreased by 21.12% (GCL) and 13.14% (INL) compared with the control group. Data are presented as the mean ± SD (n = 3). Ratios were statistically evaluated using paired student t-tests between control and experimental mice. *$p < 0.05$, **$p < 0.01$, and ***$p < 0.001$. STZ, streptozotocin; IDCK, insulin-deficient C57BL/6-Tg(pH1-siRNA$_{insulin}$/CMV-hIDE)/Korl; GCL, ganglion cell layer; INL, inner nuclear layer; ChAT, choline acetyltransferase; IR, immunoreactive; SD, standard deviation.

The density of ChAT-IR neurons was reduced in the GCL and INL in STZ-induced diabetic mice at 4–6 and 42 weeks and in IDCK mice at 20 weeks compared with that in control mice (Figs. 1,2, Table 2, **Supplementary Tables 1–3**). Compared with the findings in control mice, the number of cells in the experimental group decreased by 8.34% at 4–6 weeks (8.15% in GCL, 8.48% in INL) and by 14.89% at 42 weeks (15.73% in GCL, 14.14% in INL). Meanwhile, the cell count was 16.80% lower in IDCK mice at 20 weeks (21.12% in GCL, 13.14% in INL) than in control mice. Fig. 1 shows the representative areas in GCL and INL in control and experimental mice at approximately same retinal regions. The densities of ChAT-IR neurons in GCL and INL were lower in experimental mice than in control mice.

Table 2. Quantitative data of ChAT-IR neurons in mice in the control and experimental group.

Group	Retina	No. of ChAT-IR neurons counted (GCL)			No. of ChAT-IR neurons counted (INL)			No. of ChAT-IR neurons counted (total)		
		Experimental	Control	% Reduction	Experimental	Control	% Reduction	Experimental	Control	% Reduction
4–6 weeks STZ	Retina #1	575	611	5.89	692	750	7.73	1267	1361	6.91
	Retina #2	545	594	8.25	662	723	8.44	1207	1317	8.35
	Retina #3	540	602	10.30	626	690	9.28	1166	1292	9.75
	Mean ± SD	553 ± 19	644 ± 59	8.15 ± 2.21	660 ± 33	721 ± 30	8.48 ± 0.77	1213 ± 51	1323 ± 35	8.34 ± 1.42
42 weeks STZ	Retina #1	486	586	17.06	584	669	12.71	1070	1255	14.74
	Retina #2	531	615	13.66	594	712	16.57	1125	1327	15.22
	Retina #3	507	607	16.47	589	678	13.13	1096	1285	14.71
	Mean ± SD	508 ± 23	603 ± 15	15.73 ± 1.82	589 ± 5	686 ± 23	14.14 ± 2.12	1097 ± 28	1289 ± 36	14.89 ± 0.29
20 weeks IDCK	Retina #1	432	544	20.59	585	664	11.90	1017	1208	15.81
	Retina #2	470	575	18.26	586	698	16.05	1056	1273	17.05
	Retina #3	434	575	24.52	587	663	11.46	1021	1238	17.53
	Mean ± SD	445 ± 21	565 ± 18	21.12 ± 3.16	586 ± 1	675 ± 20	13.14 ± 2.53	1031 ± 21	1240 ± 33	16.80 ± 0.89

ChAT, choline acetyltransferase; IR, immunoreactive; GCL, ganglion cell layer; INL, inner nuclear layer; STZ, streptozotocin; SD, standard deviation; IDCK, insulin-deficient C57BL/6-Tg(pH1-siRNA$_{insulin}$/CMV-hIDE)/Korl.

Decrease of ChAT-IR neurons is more significant in GCL and INL in STZ-induced diabetic mice at 42 weeks than at 4–6 weeks (Figs. 1,2).

Fig. 2 shows the result of the paired student *t*-test in the graph. Statistically significant differences in mean density per retina between experimental and control groups in STZ-induced diabetic mice at 4–6 weeks and 42 weeks and in 20-week-old IDCK mice were identified ($p < 0.05$) (Fig. 2, **Supplementary Table 4**). At 4–6 weeks, mean ChAT-IR neuron densities were 998 ± 34 cells/mm^2 in the GCL and 1179 ± 59 cells/mm^2 in the INL in the three retinas in STZ-induced diabetic mice, whereas these values were 1076 ± 15 cells/mm^2 in the GCL and 1288 ± 54 cells/mm^2 in the INL in control mice (Fig. 2). At 42 weeks, mean ChAT-IR neuron densities were 907 ± 40 cells/mm^2 in the GCL and 1052 ± 9 cells/mm^2 in the INL in the three retinas in STZ-induced diabetic mice, whereas these values were 1076 ± 27 cells/mm^2 in the GCL and 1226 ± 40 cells/mm^2 in the INL in control mice (Fig. 2). In 20-week-old IDCK mice, mean ChAT-IR neuron densities were 795 ± 38 cells/mm^2 in the GCL and 1046 ± 2 cells/mm^2 in the INL in the three retinas, while these values were 1008 ± 32 cells/mm^2 in the GCL and 1205 ± 36 cells/mm^2 in the INL in control mice (Fig. 2).

ChAT-IR neuron distributions along the dorsoventral axis of the retina in experimental and control mice at 300 μm intervals to the optic nerve head are shown in Fig. 3. The graph shows that the pattern of the numerical distribution of ChAT-IR neurons corresponds to that of typical ChAT-IR neurons in the mouse retina described in our previous study [19]. The graph also shows that the pattern of the numerical distribution of ChAT-IR neurons of the experimental groups in the present study is quite symmetrical. The center-to-periphery gradient along the dorsoventral axis is approximately two for both INL and GCL in the control and experimental groups.

3.2 Morphological Changes in ChAT-IR Neurons in DR

Abnormal cell aggregation and cell body deformation in the retina were observed in mice with STZ-induced diabetes (Fig. 4). Fig. 4A,F show the normal cells in GCL and INL, respectively, in C57BL/6J mouse retina. Cells with round/oval cell bodies were appeared to be arranged with adequate distances. They appeared to form independently spaced retinal mosaics. In early-stage (4–6 weeks) and late-stage DR (42 weeks), some ChAT-IR neurons in the GCL (filled arrowheads in Fig. 4C–E) and INL (filled arrowhead in Fig. 4H,J) became distorted. Some other retinal cells (empty arrowheads in Fig. 4C–E) stained with DAPI were also distorted. Abnormal ChAT-IR neuron aggregation was induced by DR in the GCL (arrows in Fig. 4B,D) and INL (arrows in Fig. 4G,I), but this phenomenon was rarely observed in normal retinas.

Fig. 5 presents the dendritic morphological differences between normal (Fig. 5A) and damaged (Fig. 5B–H) ChAT-IR neurons from the retinas of control and experimental mice. The distinctive dendritic morphology of SACs has been described in many previous studies [54–57]. SACs are known to possess four or five primary dendrites that extend radially from the cell body, and dendritic arbors with many branches generally form circular dendritic fields. The dendritic arbors are concentrically and regularly distributed around the soma, and there is almost no overlap of dendritic arbors. The dendritic field has been categorized into three distinct annular zones, namely proximal, intermediate, and distal, which progress radially outward from the soma. The dendrites of the proximal and intermediate areas are relatively thin, and they taper with progression radially outward. The distal area is characterized by terminal varicosities and boutons [55]. Compared

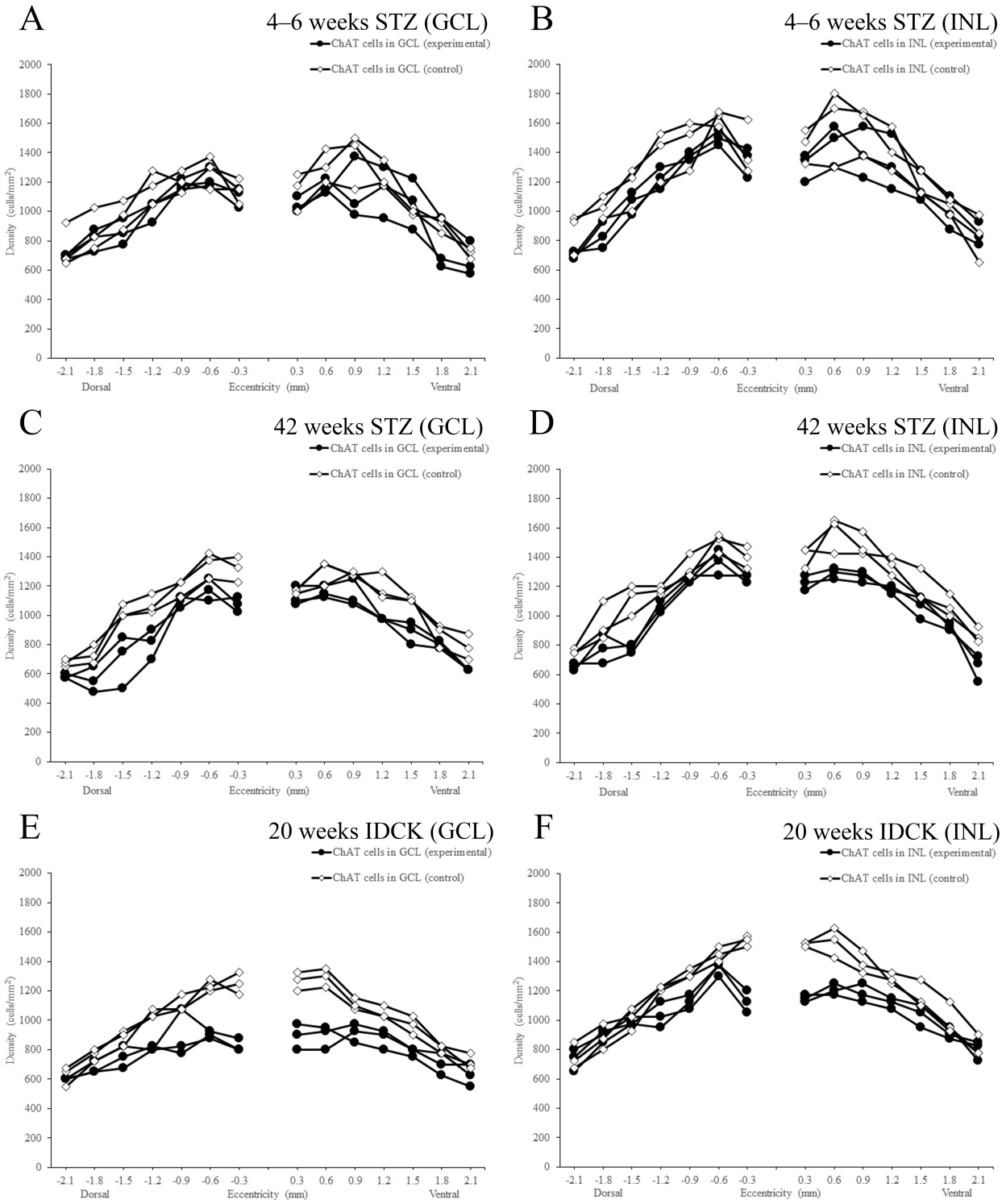

Fig. 3. Histogram of the ChAT-IR neuron distribution along the dorsoventral axis in the mouse retina. (A) ChAT-IR neurons in the GCL in control and experimental mice at 4–6 weeks after STZ injection. (B) ChAT-IR neurons in the INL in control and experimental mice at 4–6 weeks after STZ injection. (C) ChAT-IR neurons in the GCL in control and experimental mice at 42 weeks after STZ injection. (D) ChAT-IR neurons in the INL in control and experimental mice at 42 weeks after STZ injection. (E) ChAT-IR neurons in the GCL in 20-week-old IDCK control and experimental mice. (F) ChAT-IR neurons in the INL in 20-week-old IDCK control and experimental mice. The line of DR mice is located below that of normal mice on average. STZ, streptozotocin; GCL, ganglion cell layer; ChAT, choline acetyltransferase; INL, inner nuclear layer; IDCK, insulin-deficient C57BL/6-Tg(pH1-siRNA$_{insulin}$/CMV-hIDE)/Korl; IR, immunoreactive; DR, diabetic retinopathy.

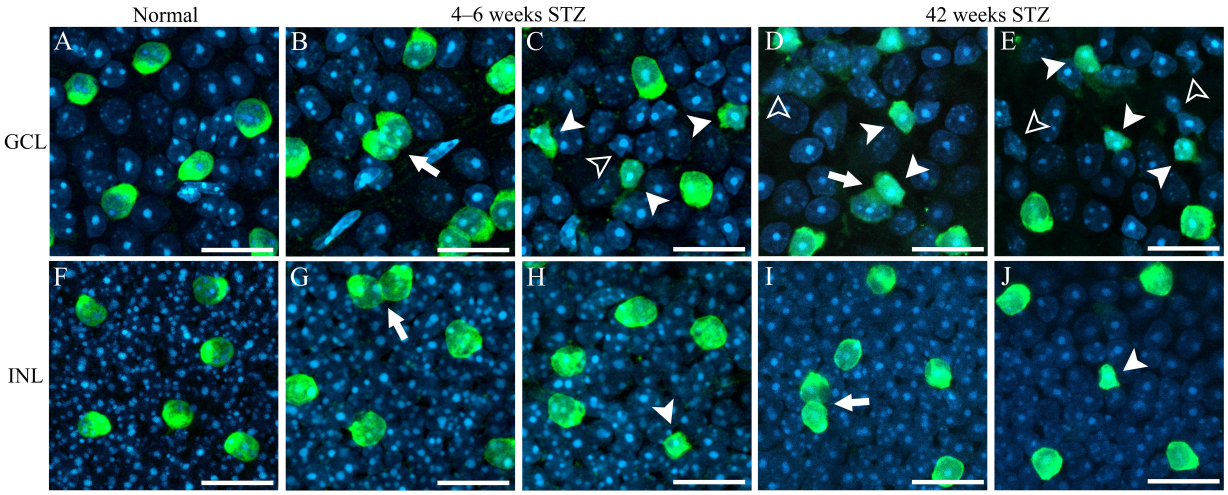

Fig. 4. High-power photomicrographs of ChAT-IR neurons. (A) Normal GCL. (B,C) GCL in retina of mice with STZ-induced diabetes at 4–6 weeks. (D,E) GCL in retina of mice with STZ-induced diabetes at 42 weeks. (F) Normal INL. (G,H) INL in retina of mice with STZ-induced diabetes at 4–6 weeks. (I,J) INL in retina of mice with STZ-induced diabetes at 42 weeks. Aggregation of ChAT-IR neurons caused by DR (arrows in panels B, D, G, and I). Distorted cell bodies of ChAT-IR neurons (filled arrowheads in panels C, D, E, H, and J). Some other retinal neurons became distorted (empty arrowheads in panels C, D, and E). STZ, streptozotocin; GCL, ganglion cell layer; INL, inner nuclear layer; ChAT, choline acetyltransferase; IR, immunoreactive; DR, diabetic retinopathy. Scale bar = 20 μm.

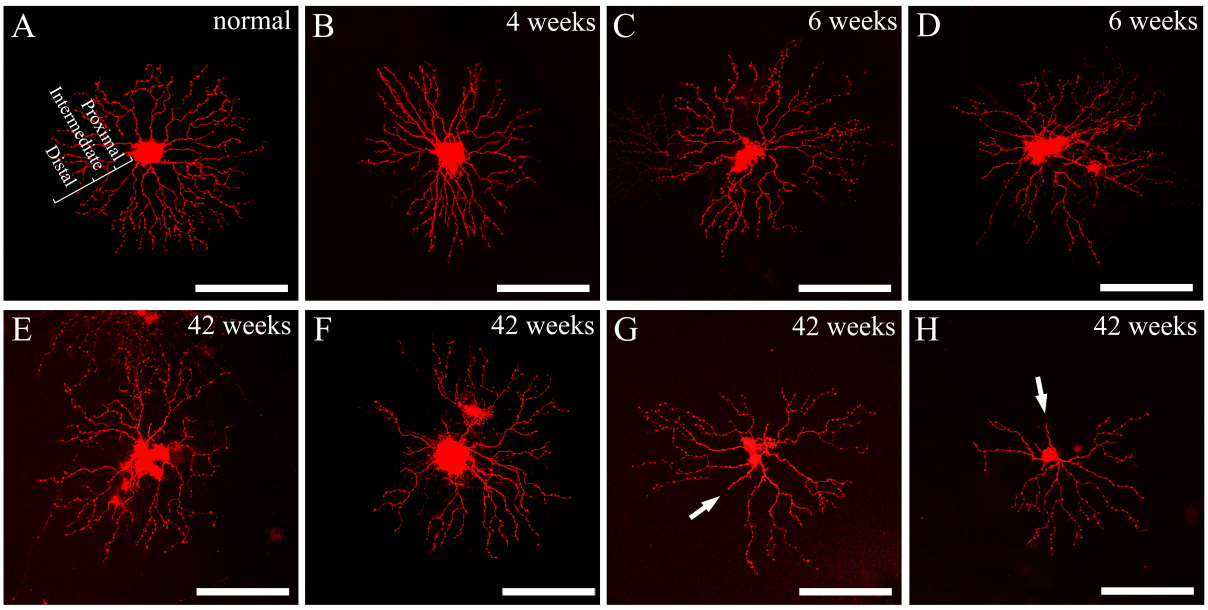

Fig. 5. Fluorescence confocal photomicrographs of DiI-injected ChAT-IR neurons. (A) Normal ChAT-IR neurons in the mouse retina. The dendritic field has been categorized three distinct annular zones: proximal, intermediate, and distal. (B) Damaged ChAT-IR neurons in STZ-induced diabetic mice at 4 weeks. (C,D) Damaged ChAT-IR neurons in STZ-induced diabetic mice at 6 weeks. (E–H) Damaged ChAT-IR neurons in STZ-induced diabetic mice at 42 weeks. Arrows indicate proximal area after the dendritic loss. ChAT, choline acetyltransferase; IR, immunoreactive; STZ, streptozotocin. Scale bar = 50 μm.

with the dendrites of normal ChAT-IR neurons, those of damaged ChAT-IR neurons in DR start to lose their regular pattern. Fig. 5B,C show the dendritic branches that lost their dendrites at 4 and 6 weeks. Fig. 5D reveals that some of the dendritic fields were clearly altered, and the dendritic branches were entangled and overlapped in space at 6 weeks. Fig. 5E,F reveal significant reductions in dendritic branches in ChAT-IR neurons at 42 weeks. The dendritic arbors varied considerably, and the deprivation of dendritic branches in the distal and intermediate areas was

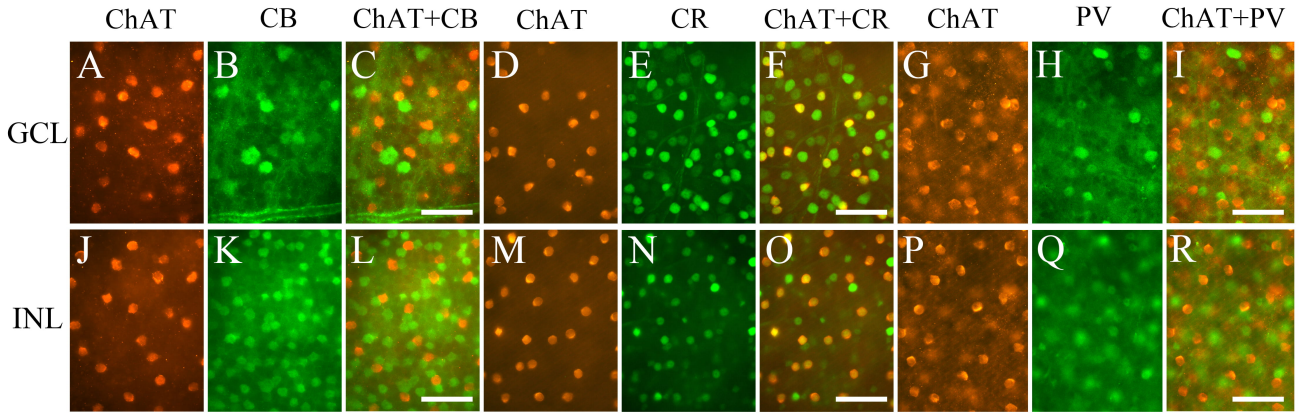

Fig. 6. Fluorescence photomicrographs of retinal whole mounts immunolabeled for ChAT and CBPs. Images of ChAT (A,D,G,J,M,P), CB (B,K), CR (E,N), and PV (H,Q). Superimposition of the images of ChAT with those of CB, CR, and PV (C,F,I,L,O,R). All ChAT-IR neurons expressed CR but not CB and PV. Panels A and B, D and E, G and H, J and K, M and N, and P and Q were photographed on the same focal plane. ChAT, choline acetyltransferase; CB, calbindin-D28K; CBP, calcium-binding protein; CR, calretinin; PV, parvalbumin; GCL, ganglion cell layer; INL, inner nuclear layer. Scale bar = 50 μm.

more obvious. Fig. 5G,H show extensively reduced dendritic branches at 42 weeks. Because of the prominent loss of terminal varicosities and boutons and the intermediate area, only the proximal zone of dendrites was observed in some cells (arrows in Fig. 5G,H).

3.3 Colocalization of ChAT and CBPs

We double-labeled ChAT with CB, CR, or PV in the mouse retina (Fig. 6). Fig. 6 shows cells expressing ChAT (Cy3), CB (FITC), CR (FITC), and PV (FITC) in both in GCL (Fig. 6A–I) and in INL (Fig. 6J–R). To confirm colocalization, we superimposed the images which were photographed at same location and same focal plane. All ChAT-IR neurons both in GCL (Fig. 6F) and INL (Fig. 6O) contained CR. No ChAT-IR neurons were colocalized with CB (Fig. 6C,L) or with PV (Fig. 6I,R).

4. Discussion

In this study, we observed changes in the density of ChAT-IR neurons in the retinas of mice with STZ-induced diabetes and IDCK mice. We also detected abnormal cell aggregation, cell body deformation, and morphological changes in dendrites caused by DR. All ChAT-IR neurons expressed CR but not CB and PV.

Amacrine cells represent the most diverse neuronal type in the retina, and approximately 30–60 different types of amacrine cells have been reported in the retina [32,58]. Of these cell types, SACs are one of the most intensively studied interneurons in the retina [59,60]. SACs can be categorized into two subpopulations based on their location (INL or GCL). In the present study, ChAT-IR neurons in retina of mouse with STZ-induced diabetes decreased total 8.34% at 4–6 weeks, and total 14.89% at 42 weeks, respectively. ChAT-IR neurons decreased total 16.80% in retina of 20-week-old IDCK mouse compared to age-matched control mouse retina. Decreased ChAT-IR neuron counts were detected in the early and late phases of DR in STZ-induced diabetic mice and in IDCK mice. In addition, the loss of these cells was greater in the late phase than in the early phase. Furthermore, the loss of ChAT-IR neurons in STZ-induced diabetic mice was slightly higher in the GCL than in the INL at 42 weeks, whereas almost no difference was detected at 4–6 weeks. The loss of ChAT-IR neurons in IDCK mice was also greater in the GCL in the present study. However, the loss of ChAT-IR neurons in 24-week-old Ins2^{AKITA} mice was greater in the INL in a previous study [17]. The functional significance of these subtle differences remains unknown. Other retinal amacrine cells, dopaminergic amacrine cells, which modulate various key visual processes, were decreased by 16.3% in the retinas of 24-week-old Ins2^{AKITA} mice compared with the control findings [17]. A previous study reported an obvious reduction in RGC counts in DR. In the retinas of STZ-induced diabetes at 10–14 weeks after the first injection, cell counts in the GCL were 20%–25% lower than the control counts [18]. In mice with STZ-induced diabetes, Brn3a-IR RGC counts in the retina were decreased by 7% at 6 weeks after the first STZ injection and those of NeuN-IR RGCs were decreased by 10% compared with the findings in control mice. In the retinas of STZ-treated mice, Brn3a-IR RGC counts in the retina were 15% lower at 12 weeks after the first injection and those of NeuN-IR RGCs were 22% lower than the control values [16]. Previous studies have also documented the apoptotic death of photoreceptors, including increased apoptosis in the outer nuclear layer and thickness reduction in the outer plexiform layer, in STZ-induced diabetic rat retina [20]. The loss of RGCs and reduced thickness of the inner plexiform layer and INL were detected in the retinas of rats with STZ-induced diabetes [21]. The present and previous data indicate that the loss of retinal

cells, including amacrine and ganglion cells, has relevance in the progression of DR.

Previous studies have noted retinal cell loss, decreased retinal thickness, and increased apoptosis in mice with STZ-induced diabetes [18]. Increased apoptosis has been demonstrated with TUNEL and caspase-3 staining in the retinas of STZ-induced diabetic rats, $Ins2^{AKITA}$ mice, and KKAY mice with type 2 diabetes [17,19]. The apoptogenic environment induced by diabetes in the human retina has been detected using apoptotic markers [61]. Also, apoptosis of RGCs in glaucoma has been shown to cause blindness [62]. Previous studies have documented that the number of retinal cells is reduced in DR and various other diseases. For example, RGC body loss and reduced SAC counts have been reported in glaucoma [63]. The number of cells in the GCL was also reduced in ischemia [64], and in the retina in Alzheimer's disease [65,66]. Thus, reduction in retinal cell counts is an apparently common symptom of diverse progressive neurodegenerative and pathologic disorders.

Abnormal aggregation and distorted cell bodies were found in ChAT-IR neurons in DR in the present study. These changes have been reported in CB-, CR-, and PV-IR neurons in the retinas of ischemic rabbits [67]. Abnormal aggregation has also been detected in some CR-IR neurons of the entorhinal cortex in Alzheimer's disease [68]. Hence, abnormal cell aggregation might represent a symptom of neurodegenerative diseases. In the present study, the length of dendrites and the number of branch points in the dendrites of ChAT-IR neurons were decreased in DR. In accordance with the present findings in the retina, the dendritic branching and spine density of neurons have been reported to be reduced in the parietal cortex of rats with diabetes [69]. The number of branch points and the total dendritic length of hippocampal CA3 pyramidal neurons were reduced in diabetic rats [70]. The total dendritic length and spine density of the pyramidal neurons of the prefrontal cortex, occipital cortex, and hippocampus were also lower in rats with diabetes [71]. Therefore, the pathological condition of DR might affect the alterations in somatic and dendritic structural elements. The reduced number of branches indicates lowered connectivity, suggesting reduced activity in the neurons.

In the present study, although abnormal aggregation, distorted cell bodies, dendritic branch loss, and SAC death were apparent in DR progression, the mechanism underlying these changes is yet to be determined. Previous studies have shown that amacrine cells die via apoptosis in DR [49]. Cell shrinkage and pyknosis are characteristic features of apoptosis and change of cytoskeleton occurs during apoptosis [72]. Thus, the morphological changes and death of SACs in the present study may be due to apoptosis. There is also a possibility that the morphological changes of SACs are due to losses of structural support of other retinal cell types. In DR, various other amacrine cell types, including dopaminergic and AII amacrine cells, and supporting glial cells were lost [2]. However, more studies are necessary to fully understand the mechanisms underlying changes and death of SACs in DR in the present study.

SACs in the retina secrete both GABA and acetylcholine. In many brain areas of mammalian species, GABAergic interneurons can be classified into subpopulations based on their expression of certain CBPs, such as CB, CR, and PV [73–75]. In the present study, all ChAT-IR neurons were expressed only in CR. Recently, transcriptomic analysis using high-throughput single-cell RNA sequencing has profiled 63 types of amacrine cells in mouse retina including SAC. They assessed the expression of ChAT including some other molecular markers in SAC but have not assessed the expression of CR to characterize the SAC [32]. It will be necessary to observe whether the CR expression in SAC agrees with single-cell genomics transcription analysis in the future. CBP expression in ChAT-IR neurons greatly differed among species [35,44–48,76,77]. In some animals, ChAT-IR neurons expressed only one of the CB [35], CR [47,77], or PV [48], whereas ChAT-IR neurons expressed two or three of CB, CR, or PV in the other animals [45,76]. The reason for various expression profiles among animals is unclear. Members of EF-hand family has different structure within their EF-hand motifs. And this structural variety provides different Ca^{2+} affinities and kinetics that affect spatiotemporal aspects of Ca^{2+} signals. Considering diverse calcium affinities, binding kinetics, and CBP buffering capacities, different physiological environments may require SACs to have different CBPs for calcium signaling pathways [42,78–80]. In addition, differential protein segregation may reflect subtle functional protein segregation in retinal visual processing and species differences [41–43,81].

Although its function is unknown, CR is a major CBP in the central visual system and has been used to label discrete neuron populations with distinctive morphology and electrophysiology in mice [52,82,83]. It has been suggested that CR is important in calcium buffering and transport similar to other CBPs, e.g., CB and PV [40,41,84,85]. CR is involved in sharpening the timing of action potentials and is associated with many biological processes, such as cell proliferation, differentiation, and cell death [85,86]. A recent study reported that CR may play a significant role in promoting synaptic efficacy during high-rate activity [87]. As SACs are important bridging cells along with direction-selective RGCs [88,89], it will be interesting to examine if CR is related to sharpening action potential timings and promoting synaptic efficacy in motion pathways.

The functional aspects of SACs in the DR have not been thoroughly investigated. Previous studies have observed that ChAT-IR neurons constituted approximately 3% of all amacrine cells in the INL and approximately 20% of all amacrine cells in the GCL, comprising one of the largest populations of amacrine cells in the retina [36,37,59,90]. This finding implies that SACs have key roles in retinal

function. In DR, the loss of SACs may cause the decrease in the optokinetic response [91]. In particular, SACs have been extensively studied as the key elements of the mechanism underlying direction selectivity, an essential neural computation that occurs in the retina for detecting a moving object [34,92,93]. Direction selectivity involves anatomically symmetric cholinergic and asymmetric GABAergic synaptic connectivity from SACs [34,87]. Thus, the loss of SACs and deprivation of dendritic branches caused by DR can interfere with direction-selective circuits in the retina. In the central visual system, diabetes disrupts functional connectivity between the primary visual cortex and higher visual regions [94]. Furthermore, diabetes causes brain atrophy, which results in a lower gray matter volume in the occipital lobe [95–97]. Therefore, these data indicate that diabetes disrupts the accuracy of visual function. However, more detailed studies are needed for understanding the impact of diabetes on vision in the retina and other visual areas.

5. Conclusions

Retinal cell death seems to be an evident clue in the progression of DR. Our results showed that the number of SACs, both in the GCL and INL, in DR mouse decreased in a time-dependent manner. Abnormal aggregation and distorted cell bodies were also found in SACs in the present study. Moreover, some of the dendritic arbors varied considerably revealing reduced and entangled dendritic branches. SACs in mouse retina expressed CR but not CB and PV. The findings of the present study are expected to contribute to a better understanding of changes of SACs in DR and may guide the development of diagnostic and therapeutic strategies for DR in the future.

Abbreviations

BGL, blood glucose level; CB, calbindin-D28K; CBP, calcium-binding protein; ChAT, choline acetyltransferase; CR, calretinin; DR, diabetic retinopathy; FITC, fluorescein isothiocyanate; GABA, gamma-aminobutyric acid; GCL, ganglion cell layer; IDCK, insulin-deficient C57BL/6-Tg(pH1-siRNA$_{insulin}$/CMV-hIDE)/Korl; INL, inner nuclear layer; IR, immunoreactive; NPDR, non-proliferative diabetic retinopathy; PB, phosphate buffer; PDR, proliferative diabetic retinopathy; PV, parvalbumin; RGC, retinal ganglion cell; SAC, starburst amacrine cell; STZ, streptozotocin.

Availability of Data and Materials

All data generated or analyzed during this study are included in this published article.

Author Contributions

JRS and CJJ designed the research study. JRS and MJL performed the research. JRS analyzed the data. JRS, MJL, and CJJ wrote the manuscript. All authors contributed to editorial changes in the manuscript. All authors read and approved the final manuscript.

Ethics Approval and Consent to Participate

All experiments involving animals were approved by the Animal Care and Use Committee of Kyungpook National University (permission no. 2020-0158).

Acknowledgment

We thank National Institute of Food and Drug Safety Evaluation for providing C57BL/6-Tg(pH1-siRNA$_{insulin}$/CMV-hIDE)/Korl mice and their information.

Funding

The work has been supported by National Research Foundation of Korea (NRF), funded by Ministry of Education (NRF-2020R1F1A1069293).

Conflict of Interest

The authors declare no conflict of interest.

Supplementary Material

Supplementary material associated with this article can be found, in the online version, at https://doi.org/10.31083/j.fbl2805092.

References

[1] Simó R, Hernández C. New Insights into Treating Early and Advanced Stage Diabetic Retinopathy. International Journal of Molecular Sciences. 2022; 23: 8513.

[2] Ren J, Zhang S, Pan Y, Jin M, Li J, Luo Y, *et al*. Diabetic retinopathy: Involved cells, biomarkers, and treatments. Frontiers in Pharmacology. 2022; 13: 953691.

[3] Wong TY, Cheung CMG, Larsen M, Sharma S, Simó R. Diabetic retinopathy. Nature Reviews. Disease Primers. 2016; 2: 16012.

[4] Cheung N, Mitchell P, Wong TY. Diabetic retinopathy. Lancet. 2010; 376: 124–136.

[5] Heng LZ, Comyn O, Peto T, Tadros C, Ng E, Sivaprasad S, *et al*. Diabetic retinopathy: pathogenesis, clinical grading, management and future developments. Diabetic Medicine. 2013; 30: 640–650.

[6] Soni D, Sagar P, Takkar B. Diabetic retinal neurodegeneration as a form of diabetic retinopathy. International Ophthalmology. 2021; 41: 3223–3248.

[7] Whitehead M, Wickremasinghe S, Osborne A, Van Wijngaarden P, Martin KR. Diabetic retinopathy: a complex pathophysiology requiring novel therapeutic strategies. Expert Opinion on Biological Therapy. 2018; 18: 1257–1270.

[8] Pearce I, Simó R, Lövestam-Adrian M, Wong DT, Evans M. Association between diabetic eye disease and other complications of diabetes: Implications for care. A systematic review. Diabetes, Obesity & Metabolism. 2019; 21: 467–478.

[9] Fowler MJ. Microvascular and macrovascular complications of diabetes. Clinical Diabetes. 2011; 29: 116–122.

[10] Simó-Servat O, Hernández C, Simó R. Diabetic Retinopathy in the Context of Patients with Diabetes. Ophthalmic Research. 2019; 62: 211–217.

[11] Karlberg C, Falk C, Green A, Sjølie AK, Grauslund J. Proliferative retinopathy predicts nephropathy: a 25-year follow-up study of type 1 diabetic patients. Acta Diabetologica. 2012; 49: 263–268.
[12] Antonetti DA, Silva PS, Stitt AW. Current understanding of the molecular and cellular pathology of diabetic retinopathy. Nature Reviews. Endocrinology. 2021; 17: 195–206.
[13] Tan GS, Cheung N, Simó R, Cheung GCM, Wong TY. Diabetic macular oedema. The Lancet. Diabetes & Endocrinology. 2017; 5: 143–155.
[14] Simó R, Stitt AW, Gardner TW. Neurodegeneration in diabetic retinopathy: does it really matter? Diabetologia. 2018; 61: 1902–1912.
[15] Solomon SD, Chew E, Duh EJ, Sobrin L, Sun JK, VanderBeek BL, *et al*. Diabetic Retinopathy: A Position Statement by the American Diabetes Association. Diabetes Care. 2017; 40: 412–418.
[16] Yang Y, Mao D, Chen X, Zhao L, Tian Q, Liu C, *et al*. Decrease in retinal neuronal cells in streptozotocin-induced diabetic mice. Molecular Vision. 2012; 18: 1411–1420.
[17] Gastinger MJ, Singh RSJ, Barber AJ. Loss of cholinergic and dopaminergic amacrine cells in streptozotocin-diabetic rat and Ins2Akita-diabetic mouse retinas. Investigative Ophthalmology & Visual Science. 2006; 47: 3143–3150.
[18] Martin PM, Roon P, Van Ells TK, Ganapathy V, Smith SB. Death of retinal neurons in streptozotocin-induced diabetic mice. Investigative Ophthalmology & Visual Science. 2004; 45: 3330–3336.
[19] Ning X, Baoyu Q, Yuzhen L, Shuli S, Reed E, Li QQ. Neuro-optic cell apoptosis and microangiopathy in KKAY mouse retina. International Journal of Molecular Medicine. 2004; 13: 87–92.
[20] Park SH, Park JW, Park SJ, Kim KY, Chung JW, Chun MH, *et al*. Apoptotic death of photoreceptors in the streptozotocin-induced diabetic rat retina. Diabetologia. 2003; 46: 1260–1268.
[21] Barber AJ, Lieth E, Khin SA, Antonetti DA, Buchanan AG, Gardner TW. Neural apoptosis in the retina during experimental and human diabetes. Early onset and effect of insulin. The Journal of Clinical Investigation. 1998; 102: 783–791.
[22] Nian S, Lo ACY, Mi Y, Ren K, Yang D. Neurovascular unit in diabetic retinopathy: pathophysiological roles and potential therapeutical targets. Eye and Vision. 2021; 8: 15.
[23] Sachdeva MM. Retinal Neurodegeneration in Diabetes: an Emerging Concept in Diabetic Retinopathy. Current Diabetes Reports. 2021; 21: 65.
[24] Wang W, Lo ACY. Diabetic Retinopathy: Pathophysiology and Treatments. International Journal of Molecular Sciences. 2018; 19: 1816.
[25] Lynch SK, Abràmoff MD. Diabetic retinopathy is a neurodegenerative disorder. Vision Research. 2017; 139: 101–107.
[26] Junod A, Lambert AE, Stauffacher W, Renold AE. Diabetogenic action of streptozotocin: relationship of dose to metabolic response. The Journal of Clinical Investigation. 1969; 48: 2129–2139.
[27] Lai AKW, Lo ACY. Animal models of diabetic retinopathy: summary and comparison. Journal of Diabetes Research. 2013; 2013: 106594.
[28] Zhang J, Wu Y, Jin Y, Ji F, Sinclair SH, Luo Y, *et al*. Intravitreal injection of erythropoietin protects both retinal vascular and neuronal cells in early diabetes. Investigative Ophthalmology & Visual Science. 2008; 49: 732–742.
[29] Feit-Leichman RA, Kinouchi R, Takeda M, Fan Z, Mohr S, Kern TS, *et al*. Vascular damage in a mouse model of diabetic retinopathy: relation to neuronal and glial changes. Investigative Ophthalmology & Visual Science. 2005; 46: 4281–4287.
[30] Anderson HR, Stitt AW, Gardiner TA, Archer DB. Diabetic retinopathy: morphometric analysis of basement membrane thickening of capillaries in different retinal layers within arterial and venous environments. The British Journal of Ophthalmology. 1995; 79: 1120–1123.
[31] Cifuentes F, Morales MA. Functional Implications of Neurotransmitter Segregation. Frontiers in Neural Circuits. 2021; 15: 738516.
[32] Yan W, Laboulaye MA, Tran NM, Whitney IE, Benhar I, Sanes JR. Mouse Retinal Cell Atlas: Molecular Identification of over Sixty Amacrine Cell Types. The Journal of Neuroscience. 2020; 40: 5177–5195.
[33] Ford KJ, Feller MB. Assembly and disassembly of a retinal cholinergic network. Visual Neuroscience. 2012; 29: 61–71.
[34] Taylor WR, Smith RG. The role of starburst amacrine cells in visual signal processing. Visual Neuroscience. 2012; 29: 73–81.
[35] Park EB, Gu YN, Jeon CJ. Immunocytochemical localization of cholinergic amacrine cells in the bat retina. Acta Histochemica. 2017; 119: 428–437.
[36] Masland RH. The many roles of starburst amacrine cells. Trends in Neurosciences. 2005; 28: 395–396.
[37] Jeon CJ, Strettoi E, Masland RH. The major cell populations of the mouse retina. The Journal of Neuroscience. 1998; 18: 8936–8946.
[38] Wei W. Neural Mechanisms of Motion Processing in the Mammalian Retina. Annual Review of Vision Science. 2018; 4: 165–192.
[39] Yoshida K, Watanabe D, Ishikane H, Tachibana M, Pastan I, Nakanishi S. A key role of starburst amacrine cells in originating retinal directional selectivity and optokinetic eye movement. Neuron. 2001; 30: 771–780.
[40] Schäfer BW, Heizmann CW. The S100 family of EF-hand calcium-binding proteins: functions and pathology. Trends in Biochemical Sciences. 1996; 21: 134–140.
[41] Baimbridge KG, Celio MR, Rogers JH. Calcium-binding proteins in the nervous system. Trends in Neurosciences. 1992; 15: 303–308.
[42] Kovács-Öller T, Szarka G, Ganczer A, Tengölics Á, Balogh B, Völgyi B. Expression of Ca^{2+}-Binding Buffer Proteins in the Human and Mouse Retinal Neurons. International Journal of Molecular Sciences. 2019; 20: 2229.
[43] Kántor O, Mezey S, Adeghate J, Naumann A, Nitschke R, Énzsöly A, *et al*. Calcium buffer proteins are specific markers of human retinal neurons. Cell and Tissue Research. 2016; 365: 29–50.
[44] Morona R, Northcutt RG, González A. Immunohistochemical localization of calbindin D28k and calretinin in the retina of two lungfishes, Protopterus dolloi and Neoceratodus forsteri: colocalization with choline acetyltransferase and tyrosine hydroxylase. Brain Research. 2011; 1368: 28–43.
[45] Cuenca N, Deng P, Linberg KA, Fisher SK, Kolb H. Choline acetyltransferase is expressed by non-starburst amacrine cells in the ground squirrel retina. Brain Research. 2003; 964: 21–30.
[46] Chandra AJ, Lee SCS, Grünert U. Melanopsin and calbindin immunoreactivity in the inner retina of humans and marmosets. Visual Neuroscience. 2019; 36: E009.
[47] Araki CM, Hamassaki-Britto DE. Calretinin co-localizes with the NMDA receptor subunit NR1 in cholinergic amacrine cells of the rat retina. Brain Research. 2000; 869: 220–224.
[48] Lee ES, Jeon CJ. Starburst amacrine cells express parvalbumin but not calbindin and calretinin in rabbit retina. Neuroreport. 2013; 24: 918–923.
[49] Feenstra DJ, Yego EC, Mohr S. Modes of Retinal Cell Death in Diabetic Retinopathy. Journal of Clinical & Experimental Ophthalmology. 2013; 4: 298.
[50] Fajardo RJ, Karim L, Calley VI, Bouxsein ML. A review of rodent models of type 2 diabetic skeletal fragility. Journal of Bone

and Mineral Research. 2014; 29: 1025–1040.
[51] Lee ES, Kim TJ, Jeon CJ. Identification of parvalbumin-containing retinal ganglion cells in rabbit. Experimental Eye Research. 2013; 110: 113–124.
[52] Lee ES, Lee JY, Jeon CJ. Types and density of calretinin-containing retinal ganglion cells in mouse. Neuroscience Research. 2010; 66: 141–150.
[53] Kim TJ, Jeon CJ. Morphological classification of parvalbumin-containing retinal ganglion cells in mouse: single-cell injection after immunocytochemistry. Investigative Ophthalmology & Visual Science. 2006; 47: 2757–2764.
[54] Keeley PW, Whitney IE, Raven MA, Reese BE. Dendritic spread and functional coverage of starburst amacrine cells. The Journal of Comparative Neurology. 2007; 505: 539–546.
[55] Masland RH, Tauchi M. The cholinergic amacrine cell. Trends in Neurosciences. 1986; 9: 218–223.
[56] Tauchi M, Masland RH. Local order among the dendrites of an amacrine cell population. The Journal of Neuroscience. 1985; 5: 2494–2501.
[57] Tauchi M, Masland RH. The shape and arrangement of the cholinergic neurons in the rabbit retina. Proceedings of the Royal Society of London. Series B, Biological Sciences. 1984; 223: 101–119.
[58] Masland RH. Neuronal cell types. Current Biology. 2004; 14: R497–500.
[59] Grünert U, Martin PR. Cell types and cell circuits in human and non-human primate retina. Progress in Retinal and Eye Research. 2020; 100844.
[60] Balasubramanian R, Gan L. Development of Retinal Amacrine Cells and Their Dendritic Stratification. Current Ophthalmology Reports. 2014; 2: 100–106.
[61] Abu-El-Asrar AM, Dralands L, Missotten L, Al-Jadaan IA, Geboes K. Expression of apoptosis markers in the retinas of human subjects with diabetes. Investigative Ophthalmology & Visual Science. 2004; 45: 2760–2766.
[62] Cordeiro MF, Migdal C, Bloom P, Fitzke FW, Moss SE. Imaging apoptosis in the eye. Eye. 2011; 25: 545–553.
[63] Cooley-Themm CA, Ameel Q, Linn DM, Linn CL. Loss of displaced starburst amacrine cells in a rat glaucoma model. Journal of Ophthalmic Research and Ocular Care. 2017; 1: 28–38.
[64] Tong N, Zhang Z, Gong Y, Yin L, Wu X. Diosmin protects rat retina from ischemia/reperfusion injury. Journal of Ocular Pharmacology and Therapeutics: the Official Journal of the Association for Ocular Pharmacology and Therapeutics. 2012; 28: 459–466.
[65] Marziani E, Pomati S, Ramolfo P, Cigada M, Giani A, Mariani C, *et al*. Evaluation of retinal nerve fiber layer and ganglion cell layer thickness in Alzheimer's disease using spectral-domain optical coherence tomography. Investigative Ophthalmology & Visual Science. 2013; 54: 5953–5958.
[66] Blanks JC, Torigoe Y, Hinton DR, Blanks RH. Retinal pathology in Alzheimer's disease. I. Ganglion cell loss in foveal/parafoveal retina. Neurobiology of Aging. 1996; 17: 377–384.
[67] Kwon OJ, Kim JY, Kim SY, Jeon CJ. Alterations in the localization of calbindin D28K-, calretinin-, and parvalbumin-immunoreactive neurons of rabbit retinal ganglion cell layer from ischemia and reperfusion. Molecules and Cells. 2005; 19: 382–390.
[68] Mikkonen M, Alafuzoff I, Tapiola T, Soininen H, Miettinen R. Subfield- and layer-specific changes in parvalbumin, calretinin and calbindin-D28K immunoreactivity in the entorhinal cortex in Alzheimer's disease. Neuroscience. 1999; 92: 515–532.
[69] Malone JI, Hanna S, Saporta S, Mervis RF, Park CR, Chong L, *et al*. Hyperglycemia not hypoglycemia alters neuronal dendrites and impairs spatial memory. Pediatric Diabetes. 2008; 9: 531–539.
[70] Magariños AM, McEwen BS. Experimental diabetes in rats causes hippocampal dendritic and synaptic reorganization and increased glucocorticoid reactivity to stress. Proceedings of the National Academy of Sciences of the United States of America. 2000; 97: 11056–11061.
[71] Martínez-Tellez R, Gómez-Villalobos MDJ, Flores G. Alteration in dendritic morphology of cortical neurons in rats with diabetes mellitus induced by streptozotocin. Brain Research. 2005; 1048: 108–115.
[72] Elmore S. Apoptosis: a review of programmed cell death. Toxicologic Pathology. 2007; 35: 495–516.
[73] Qi Y, Cheng H, Wang Y, Chen Z. Revealing the Precise Role of Calretinin Neurons in Epilepsy: We Are on the Way. Neuroscience Bulletin. 2022; 38: 209–222.
[74] Druga R. Neocortical inhibitory system. Folia Biologica. 2009; 55: 201–217.
[75] Reynolds GP, Abdul-Monim Z, Neill JC, Zhang ZJ. Calcium binding protein markers of GABA deficits in schizophrenia–postmortem studies and animal models. Neurotoxicity Research. 2004; 6: 57–61.
[76] Morona R, Moreno N, López JM, González A. Comparative analysis of calbindin D-28K and calretinin in the retina of anuran and urodele amphibians: Colocalization with choline acetyltransferase and tyrosine hydroxylase. Brain Research. 2007; 1182: 34–49.
[77] Gábriel R, Witkovsky P. Cholinergic, but not the rod pathway-related glycinergic (All), amacrine cells contain calretinin in the rat retina. Neuroscience Letters. 1998; 247: 179–182.
[78] Gifford JL, Walsh MP, Vogel HJ. Structures and metal-ion-binding properties of the Ca2+-binding helix-loop-helix EF-hand motifs. The Biochemical Journal. 2007; 405: 199–221.
[79] Hackney CM, Mahendrasingam S, Penn A, Fettiplace R. The concentrations of calcium buffering proteins in mammalian cochlear hair cells. The Journal of Neuroscience. 2005; 25: 7867–7875.
[80] Nägerl UV, Novo D, Mody I, Vergara JL. Binding kinetics of calbindin-D(28k) determined by flash photolysis of caged Ca(2+). Biophysical Journal. 2000; 79: 3009–3018.
[81] Hamano K, Kiyama H, Emson PC, Manabe R, Nakauchi M, Tohyama M. Localization of two calcium binding proteins, calbindin (28 kD) and parvalbumin (12 kD), in the vertebrate retina. The Journal of Comparative Neurology. 1990; 302: 417–424.
[82] Camillo D, Ahmadlou M, Saiepour MH, Yasaminshirazi M, Levelt CN, Heimel JA. Visual Processing by Calretinin Expressing Inhibitory Neurons in Mouse Primary Visual Cortex. Scientific Reports. 2018; 8: 12355.
[83] Park HJ, Kong JH, Kang YS, Park WM, Jeong SA, Park SM, *et al*. The distribution and morphology of calbindin D28K- and calretinin-immunoreactive neurons in the visual cortex of mouse. Molecules and Cells. 2002; 14: 143–149.
[84] Polans A, Baehr W, Palczewski K. Turned on by Ca2+! The physiology and pathology of Ca(2+)-binding proteins in the retina. Trends in Neurosciences. 1996; 19: 547–554.
[85] Rogers JH. Calretinin: a gene for a novel calcium-binding protein expressed principally in neurons. The Journal of Cell Biology. 1987; 105: 1343–1353.
[86] Schwaller B. Calretinin: from a "simple" Ca(2+) buffer to a multifunctional protein implicated in many biological processes. Frontiers in Neuroanatomy. 2014; 8: 3.
[87] Zhang C, Wang M, Lin S, Xie R. Calretinin-Expressing Synapses Show Improved Synaptic Efficacy with Reduced Asynchronous Release during High-Rate Activity. The Journal of Neuroscience. 2022; 42: 2729–2742.
[88] Pottackal J, Singer JH, Demb JB. Receptoral Mechanisms for Fast Cholinergic Transmission in Direction-Selective Retinal Circuitry. Frontiers in Cellular Neuroscience. 2020; 14: 604163.

[89] Ray TA, Roy S, Kozlowski C, Wang J, Cafaro J, Hulbert SW, *et al*. Formation of retinal direction-selective circuitry initiated by starburst amacrine cell homotypic contact. ELife. 2018; 7: e34241.
[90] Pérez De Sevilla Müller L, Shelley J, Weiler R. Displaced amacrine cells of the mouse retina. The Journal of Comparative Neurology. 2007; 505: 177–189.
[91] Baya Mdzomba J, Joly S, Rodriguez L, Dirani A, Lassiaz P, Behar-Cohen F, *et al*. Nogo-A-targeting antibody promotes visual recovery and inhibits neuroinflammation after retinal injury. Cell Death & Disease. 2020; 11: 101.
[92] Pottackal J, Singer JH, Demb JB. Computational and Molecular Properties of Starburst Amacrine Cell Synapses Differ With Postsynaptic Cell Type. Frontiers in Cellular Neuroscience. 2021; 15: 660773.
[93] Chen Q, Pei Z, Koren D, Wei W. Stimulus-dependent recruitment of lateral inhibition underlies retinal direction selectivity. ELife. 2016; 5: e21053.
[94] Qi CX, Huang X, Tong Y, Shen Y. Altered Functional Connectivity Strength of Primary Visual Cortex in Subjects with Diabetic Retinopathy. Diabetes, Metabolic Syndrome and Obesity: Targets and Therapy. 2021; 14: 3209–3219.
[95] Zhang T, Shaw M, Cherbuin N. Association between Type 2 Diabetes Mellitus and Brain Atrophy: A Meta-Analysis. Diabetes & Metabolism Journal. 2022; 46: 781–802.
[96] Filip P, Canna A, Moheet A, Bednarik P, Grohn H, Li X, *et al*. Structural Alterations in Deep Brain Structures in Type 1 Diabetes. Diabetes. 2020; 69: 2458–2466.
[97] Ferreira FS, Pereira JMS, Reis A, Sanches M, Duarte JV, Gomes L, *et al*. Early visual cortical structural changes in diabetic patients without diabetic retinopathy. Graefe's Archive for Clinical and Experimental Ophthalmology. 2017; 255: 2113–2118.